Atmospheric Environment 238 (2020) 117745

Contents lists available at ScienceDirect

Atmospheric Environment

journal homepage: http://www.elsevier.com/locate/atmosenv

Size-differentiated patterns of exposure to submicron particulate matter across regions and seasons in China

Ming Liu [a], Rebecca K. Saari [a,b,**], Gaoxiang Zhou [a,c], Xiangnan Liu [c], Jonathan Li [a,d,*]

[a] Department of Geography and Environmental Management, University of Waterloo, Waterloo, Ontario, N2L 3G1, Canada
[b] Department of Civil and Environmental Engineering, University of Waterloo, Waterloo, Ontario, N2L 3G1, Canada
[c] School of Information Engineering, China University of Geosciences, Beijing, 100083, China
[d] Fujian Key Laboratory of Sensing and Computing for Smart Cities, School of Informatics, Xiamen University, Xiamen, FJ, 361005, China

HIGHLIGHTS

- Satellite AOD and aerosol optical-mass relationships yield size-resolved exposure.
- Chinese population on average was exposed to submicron sized particles in 2017.
- Easterners more exposed to small particles, especially in warm seasons.
- Region with high mass concentration also had smallest mean particle size.

ARTICLE INFO

Keywords:
Air pollution
Exposure
Particle size
Satellite retrieval
Particulate matter
China

ABSTRACT

Air pollution in China has reached unprecedented levels due to rapid economic and industrial development. More than 90% of Chinese population experience higher health risks attributable to ambient fine particulate matter ($PM_{2.5}$) exposure. Although evidence suggests that particle size may be an effect modifier on $PM_{2.5}$-related health risks, few studies have explored this due to lack of size-resolved exposure data. In this study, we derive size-resolved particle effective radius of $PM_{2.5}$ using theoretical relationships between aerosol microphysical characteristics and satellite optical measurements to explore the spatial variability and population exposure to ambient particle size. Applying this method to China in 2017, we observed annual mean effective radii between 0.3 and 1.3 μm with a mean average error of 0.1 μm. We find that 1% or less of the Chinese population was exposed to annual $PM_{2.5}$ concentrations less than 10 $\mu g/m^3$ and a mean particle effective radius greater than 0.7 μm (i.e. aerodynamic diameter of PM_1). Spatially, the Centre economic region had the highest annual-mean $PM_{2.5}$ exposures, where 90% of the population was exposed to concentrations higher than 50 $\mu g/m^3$ and 98% was exposed to particles with mean radius below 0.5 μm. Temporally, although the highest $PM_{2.5}$ concentrations were more likely to occur in winter, summertime was the season during which the highest percentage of the national population (86%) lived in the regions in which the fine fraction had the smallest mean particle radii (<0.5 μm). This study demonstrates the potential of remote sensing techniques to enable large-scale $PM_{2.5}$ estimation, including concentrations and sizes. The revealed prevalence of exposure to PM_1, and lack of particle size validation data, motivate further research to better understand size-resolved exposures and impacts of $PM_{2.5}$ at population scales.

1. Introduction

Exposure to ambient atmospheric pollutants, especially fine particulate matter ($PM_{2.5}$), has been shown to significantly increase the risk of mortality from cardiovascular and respiratory illnesses (Pope et al., 2018; Sacks et al., 2011). China has suffered from severe $PM_{2.5}$ pollution with its rapid economic development and industrialization. In 2017, approximately 0.85 million premature death and 19.8 million disability-adjusted life-years (DALYs) lost were reported to be attributable to ambient $PM_{2.5}$ exposure in China, accounting for 29% of the

* Corresponding author. Department of Geography and Environmental Management, University of Waterloo, Waterloo, Ontario, N2L 3G1, Canada.
** Corresponding author. Department of Civil and Environmental Engineering, University of Waterloo, Waterloo, Ontario, N2L 3G1, Canada.
E-mail addresses: rebecca.saari@uwaterloo.ca (R.K. Saari), junli@uwaterloo.ca (J. Li).

https://doi.org/10.1016/j.atmosenv.2020.117745
Received 31 December 2019; Received in revised form 11 June 2020; Accepted 25 June 2020
Available online 29 June 2020

$PM_{2.5}$-related premature deaths and 24% of the DALYs worldwide (Cohen et al., 2017). While epidemiologic relationships have been established for $PM_{2.5}$ mass concentrations and a variety of health endpoints, other particulate characteristics, like composition and size, may be relevant in informing such relationships, e.g., via effect modification, or in identifying new ones. Size-resolved particular matter observations are thus pertinent for exposure assessment. Here, we aim to provide national population-scale size-resolved exposures to $PM_{2.5}$.

Using various exposure methods, previous toxicological and epidemiological studies found that particles with different size ranges have independent effects on human health (Esposito et al., 2012; Gerlofs--Nijland et al., 2009). Small particles can penetrate into the airways and alveoli, and finally into the bloodstream and cardiovascular system, leading to inflammation and oxidative stress (Delfino et al., 2005; Mills et al., 2009). Smaller particles may have higher toxicity since the relatively large number and surface area of small particles may increase their risk of absorbing toxic substances (Hoek et al., 2009; Ostro et al., 2015; Samoli et al., 2016).

Despite such work indicating the significance of size, the scale of current size-resolved exposure and epidemiological studies is limited in terms of the exposed population, as well as spatial and temporal domains. This is due primarily to typical exposure measurement techniques, including fixed ground-based stations (Chen et al., 2017; Hu et al., 2018) and personal portable monitors (Gulliver and Briggs, 2007; Pacitto et al., 2018; Yu et al., 2012). Personal exposure monitors provide crucial individual-level detail and insights. Nonetheless, supplementary population-level exposures can inform individual-level studies, and may offer their own unique insights given the nature of environmental exposures (Pekkanen and Pearce, 2001). Population-scale studies that involve some size-resolution in the fine fraction are primarily limited to station-based measurements, the spatial continuity and coverage of which are limited due to their high costs of station construction, operation and maintenance (Kumar et al., 2015). Wichmann et al. (2000) used measurements from a single monitoring station to assess particle exposure in Erfurt, Germany, with a population of approximately 200, 000 people, indicating that exposure to ambient concentrations of fine and ultrafine particles had comparable effects. Lin et al. (2016) found the excess risk (ER) of cardiovascular mortality with PM_1 was 6.48% (95% CI: 2.10%, 11.06%), higher than those associated with PM_{10} and $PM_{2.5}$ reported in their study, demonstrating that PM_1 might be an important characteristic of particulate matter pollution attributable to cardiovascular mortality in Guangzhou, China. Two monitoring stations were used in this study.

The distribution of ambient particles shows variability, reflecting regional variations in aerosol emissions, transport and physicochemical processes (Pinto et al., 2004; Wang et al., 2013; Yang et al., 2018). Chen *et al.* (2018b) showed the station-based spatial distributions of PM_1 and $PM_{2.5}$ concentrations and the seasonal variations of the $PM_1/PM_{2.5}$ ratio the provincial level, demonstrating the spatial and temporal variability of size-fractioned particulate matter particles. Thus, exposure estimates based on in-situ measurements in a sparse monitoring network cannot fully represent the average exposure of the whole city population, especially, perhaps, for ultrafine particles (Pekkanen and Kulmala, 2004), potentially limiting their use for population-based studies. Kodros et al. (2018, 2016) indicated that particle size measurements in polluted areas, such as India and China, are especially limited, leading to uncertainties.

Many techniques are used to address the limited spatial coverage of fixed site measurements of particulate matter exposure based on multiple data sources. Ground-based measurements may be used to validate alternative estimates from numerical models and data-driven techniques (Knibbs et al., 2018; Ma et al., 2014; Xiao et al., 2018). These approaches differ in their current level of application to size-resolved exposure estimates. Numerical chemical transport models offer an approach to obtain aerosol components and behavior with a relatively high spatio-temporal resolution and coverage (Brauer et al., 2012; Saari et al., 2019). Further, they are capable of providing size-resolved exposures, as in Kodros et al., (2018); however, the application thereof remains limited as the use of size-resolved aerosol schemes greatly increases computational cost of simulations (Kodros and Pierce, 2017). Data-driven techniques are beginning to offer size-related information through the advent of novel and relatively low-cost particle-counting sensors. While such sensors do not provide size-resolved mass concentrations, particle number concentration can be related to the mass distributions. Recent work, reviewed and advanced in Saha et al., (2019), employed short-term fixed-site measurements to develop land use regression models of particle number concentration – a proxy for ultrafine exposure. Satellite remote sensing techniques have been applied to obtain concentrations of air pollutants with relatively with high spatial coverage (van Donkelaar et al., 2016; Yan et al., 2017). Zhang and Li (2015) established a theoretical relationship between fine particulate mass and satellite measurement based on aerosol microphysical behaviors. However, these methods have less commonly been applied to derive particle size (Hilboll et al., 2013; Larkin et al., 2017). Aside from the Angstrom Exponent (AE), which is inversely related to aerosol size (Qi et al., 2013; Wang et al., 2013), there is little information available on particle size, especially for submicron exposures at a population scale.

The objective of this study is to reveal the extent of $PM_{2.5}$ exposure by particle size in the submicrometer range. To achieve this, we employed a spatial statistical model for $PM_{2.5}$ mass concentration retrieval and then combined aerosol microphysical characteristics with satellite optical measurements to estimate the ground-level particle effective radius of $PM_{2.5}$. We applied this to examine the geographic variability and population exposure of the PM2.5 size-resolved mass concentrations over China in 2017. The uncertainty of our estimates is also discussed.

2. Materials and methods

2.1. Satellite-retrieved $PM_{2.5}$ estimation

Ground-level $PM_{2.5}$ concentrations were estimated based on satellite and meteorological data using a Geographically Weighted Regression (GWR) model which were widely adopted for PM2.5 concentrations retrievals (Supplementary Material Part 9). Prior to GWR modelling, we corrected satellite-observed columnar aerosol optical depth (AOD) at the wavelength of 550 nm into ground-level extinction (b_{ext}) based on an assumption that the majority of atmospheric aerosols evenly suspend in the planetary boundary layer (PBL) due to the active mixing (Kaufman et al., 2003). Fine mode AOD was adopted based on a look-up table–-spectral deconvolution algorithm, which was found to be closely related to $PM_{2.5}$ (Yan et al., 2017; Zhang and Li, 2015). Hygroscopic growth functions were employed since aerosol hygroscopic characteristics affect extinction by changing the particle size. The correction formula is given below:

$$b_{ext,dry} = \frac{\eta b_{ext}}{f(RH)} = \frac{\eta \tau}{Hf(RH)} \quad (1)$$

where $b_{ext,dry}$ refers to extinction coefficient of fine particles under dry conditions; η refers to fine mode fraction; τ refers to satellite-derived AOD at 550 nm; H refers to the height of PBL; f (RH) refers to a hygroscopic growth function with independent variables of relative humidity (RH), which are calculated based on the previous studies (Chen et al., 2014, 2015; Liu et al., 2019a; Yan et al., 2017).

In addition to aerosol extinction, we include meteorological parameters expected to be associated the generation, accumulation, and removal of aerosols, including air temperature (T) (Day and Pandis, 2011; Liu et al., 2007), surface wind speed (WS) (Zhou et al., 2015), horizontal visibility (V) (Xiao et al., 2018; You et al., 2016) and elevation (DEM) (Wang et al., 2018). These variables have been employed

previously in studies with acceptable performance (He and Huang, 2018; Kloog et al., 2012; Liu et al., 2009; Ma et al., 2016, 2014). We considered and excluded additional variables, such as pressure, that did not independently improve performance (details in Supplementary Material Section 7). We employ these variables to estimate PM2.5 across China using the GWR model, according to the following model structure:

$$PM_{2.5(i,j)} = \beta_{0(i,j)} + \beta_{b_{ext,dry}\ (i,j)} b_{ext,dry\ (i,j)} + \beta_{T(i,j)} T_{(i,j)} + \beta_{WS(i,j)} WS_{(i,j)} + \beta_{V(i,j)} V_{(i,j)} + \beta_{DEM(i,j)} DEM_{(i,j)} + \varepsilon_{(i,j)} \quad (2)$$

where $PM_{2.5(i,j)}$ is the ground-level $PM_{2.5}$ concentration at location (i, j); β_0 is the intercept; β with different subscripts denote the slope of corresponding variables. $\varepsilon_{(i,j)}$ is the error term at location (i,j). Gaussian distance decay functions were adopted to determine the weights. Considering spatial autocorrelation, 10-fold block cross validation (CV) was adopted to evaluate the model performance (Roberts et al., 2017). Four metrics, including the determination coefficient (R^2), root mean square error (RMSE), mean absolute error (MAE) and mean bias error (MBE), were used to compare the retrieved and measured values. The variance inflation factor (VIF) was employed to measure the collinearity of the adopted variables (Table S5). It was less than 3 for all variables, indicating low collinearity.

The detailed description of adopted parameters in above formulas is shown in Table 1 and in the Supplementary Material. All independent data were masked before resampling to 3 km using the cubic convolution algorithm and were unified with respect to coordinate system and data format, following the geophysical coverage of China and spatial resolution of MODIS AOD.

2.2. Particle size calculation

The aerosol radius was calculated with ground-level mass concentrations based on optical-mass theoretical relationships (Liu et al., 2019b). We assumed aerosol particles were homogeneous spheres to statistically describe an ensemble of particles due to the aerosol complexity in terms of composition and geometry (Holben et al., 1998; Nakajima et al., 1996). The lognormal distribution was adopted to express the particle size distribution, which can be described by two parameters: geometric mean radius (r_g) and geometric standard deviation (σ_g). Since aerosol extinction is proportional to r^2, we used the effective particle radius (r_e), a weighted mean of size distribution, to represent the particle size according to the rule of lognormal distribution.

$$r_e = \frac{\int_0^\infty r^3 n(r)\mathrm{d}r}{\int_0^\infty r^2 n(r)\mathrm{d}r} = r_g \exp\left(\frac{5\ln^2\sigma_g}{2}\right) \quad (3)$$

Table 1
Detailed data description.

Data (Unit)	Spatial resolution	Descriptive statistics of collocated data		
		Min	Max	Mean
$PM_{2.5}$ (μg/m^3)	–	1.00	736.25	45.55
AOD (Unitless)	3 km; 10 km	0.03	3.86	0.47
T (K)	0.25°	260.81	309.67	289.04
WS (m/s)	0.25°	0.16	15.82	3.49
RH (%)	0.25°	9.04	96.83	56.93
PBLH (m)	0.25°	25.90	6328.97	1837.02
V (km)	–	0.26	49.99	9.45
DEM (m)	1 km	−13.46	4553.22	370.51

Note: Ground-level PM2.5 concentrations were obtained from China National Environment Monitoring Center; AOD images obtained from NASA Atmosphere Archive and Distribution System; T, WS, RH, and PBLH were obtained from NCEP GDAS/FNL 0.25 Degree Global Tropospheric Analyses and Forecast Grids; V was obtained from NCEP ADP Global Surface Observational Weather Data; DEM was obtained from Resources and Environmental Science Data Center. The detailed descriptions were provided in Supplementary Material.

where $n(r)$ is the lognormal size distribution of accumulation mode aerosol; σ_g was set at 2, which refers to the general range of different fine particles (Reid et al., 2003; Steele et al., 2006).

Consequently, the columnar particle mass concentration (M) and $b_{ext,dry}$ can physically be defined and deduced:

$$\mathrm{M} = \frac{4}{3}\pi\rho\mathrm{H}\int \mathrm{r}^3\mathrm{n}(\mathrm{r})\mathrm{dr} = \frac{4}{3}\pi\rho\mathrm{H}r_g^3 \exp\left(\frac{9\ln^2\sigma_g}{2}\right) \quad (4)$$

$$\mathrm{b}_{ext,dry} = \frac{\eta}{f(RH)}\int_0^\infty \mathrm{Q}_{ext}\pi\mathrm{r}^2\mathrm{n}(\mathrm{r})\mathrm{dr} \quad (5)$$

where ρ is the mean bulk density of atmospheric particles, with a constant value of 1.5 g/cm^3 (Clarisse et al., 2010; Li et al., 2016), Q_{ext} is the extinction efficiency, which is related to visibility (Koschmieder, 1924),

$$\mathrm{Q}_{ext} = \frac{3.912/\mathrm{V}}{\pi(r_e)^2\exp(-3\ln^2\sigma_g)} \quad (6)$$

Equating with Eqs. (1) and (3) – (6) yields,

$$\mathrm{r}_e = \left(\frac{3\mathrm{M}(3.912/\mathrm{V})}{4\pi\rho\tau\exp(-3\ln^2\sigma_g)}\right)^{1/3} \quad (7)$$

In Eq. (7), M was calculated based on the GWR model in Section 2.1; τ and V are spatial variables acquired from satellite and re-analysis datasets. The ρ and σ_g were treated as constants, the effect of which is examined in Section 4.

2.3. Population data

Gridded population data with a spatial resolution of 1 km were obtained for 2015 from "Resource and Environmental Science Data Center of the Chinese Academy of Sciences (RESDC) (http://www.resdc.cn/)". This dataset provided 1 km gridded population using multi-factor weighting based on county-level demographic data, considering land use type, nighttime light intensity and residential density (Xu, 2017). The annual population in 2017 in each province was also acquired from the "Chinese National Bureau of Statistics (http://www.stats.gov.cn/tjsj/ndsj/)" to project the gridded 2015 population to 2017. To project the gridded data, the ratio of the gridded population to the whole population in each province in 2015 was first calculated. The gridded population in 2017 was then obtained by multiplying this ratio in each province by the whole population in the corresponding province in 2017. The final gridded population was resampled to 3 km to match the spatial resolution of estimated $PM_{2.5}$ concentrations and sizes.

3. Results

3.1. Ground-level $PM_{2.5}$ concentration estimation

As mentioned in Section 2.1, the GWR model was established using ground-based $PM_{2.5}$ measurements with a total of 176,385 available samples. Table 2 shows the results of model fitting and cross validation based on the GWR model. The model fitting R^2 between the estimated and measured $PM_{2.5}$ mass concentration is 0.82, with RMSE of 15.7 μg/m^3 and MAE of 10.1 μg/m^3. A negative MBE suggests $PM_{2.5}$ concentrations were underestimated by −6.63 μg/m^3. Compared to the model fitting results, the CV R^2 (0.80) decreases by only 0.04 and the CV RMSE increases by 2.3 μg/m^3, indicating that there is no substantial overfitting in the model. Both overall R^2 and CV R^2 are higher than 0.80, showing that the accuracy of $PM_{2.5}$ estimation results are acceptable. In addition, as shown in Fig. 1a, the spatial pattern of annual mean $PM_{2.5}$ estimation appears to be visually consistent with that of ground observations in 2017. The concentrations in eastern China are generally higher than those in the west, except for the Taklamakan Desert. As designated by Chinese National Bureau of Statistics (http://www.stats.gov.cn/tjsj/nd

Table 2
Validation of daily $PM_{2.5}$ estimates.

	R^2	RMSE ($\mu g/m^3$)	MAE ($\mu g/m^3$)	MBE ($\mu g/m^3$)	N	Equations
Model-fitting	0.82	15.7	10.1	−6.6	176,385	y = 0.81x+14.32
CV	0.80	18.0	11.9	−6.0	176,385	y = 0.80x+15.89

Note: N: sample numbers; R^2: determination coefficient; RMSE: root-mean-square error; MAE: mean absolute error; MBE: mean bias error.

sj/2017/indexeh.htm), we divided the entire study area into four regions (East, West, Northeast and Centre) based on their economic development (Fig. 1b). The East is the most developed region in China, contributing 52.6% of overall GDP, while the Northeast has the smallest GDP, accounting for 6% of the total. The highest annual-mean growth rates of GDP and industrial added value occurred in the Centre region, with respective values of 10.8% and 12.5%, respectively (2006–2017).

Results in Fig. 1 show that the highest annual-mean $PM_{2.5}$ levels were observed in the Centre, with a mean concentration of 54.3 $\mu g/m^3$, followed by the West, the East, and the Northeast region. Although the East had the second lowest $PM_{2.5}$ levels, hotspots in the Beijing-Tianjin-Hebei (BTH) metropolitan region experienced high $PM_{2.5}$ exposures, with concentrations exceeding 55 $\mu g/m^3$. Elevated $PM_{2.5}$ concentrations in the West were located in the Tarim Basin (Taklamakan Desert), the Guanzhong Plain, and the Sichuan Basin. The seasonal variations of $PM_{2.5}$ concentrations are shown in the Supplementary Material, indicating that winter was the most polluted season in 2017, with a mean value of 61.1 $\mu g/m^3$. Following van Donkelaar et al. (2016), exposed population counts and cumulative distributions of $PM_{2.5}$ concentrations by population for different regions are shown in Fig. 2. The national population-weighted average (PWA) of ambient $PM_{2.5}$ is estimated to have been 52.1 $\mu g/m^3$ in 2017. The highest PWA concentration was observed in the Centre (60.9 $\mu g/m^3$), while the Northeast had the lowest value (38.4 $\mu g/m^3$). The standard deviation (STD) of PWA in these two regions was below 20 $\mu g/m^3$, indicating a mean separation of at least one STD between them. The PWA concentrations in the West (46.9 $\mu g/m^3$) were lower than those in the East (53.9 $\mu g/m^3$), although this order is reversed for mass concentrations. The West and East had significantly higher STDs than the other regions, with the respective values of 96.2 $\mu g/m^3$ and 39.9 $\mu g/m^3$, indicating highly variable exposures.

The cumulative distribution of population exposure to mass concentrations was also explored to describe the percentage of population experiencing high PM2.5 levels (Fig. 2b). The results show 12.3% of the Chinese population living where concentrations meet the China national ambient air quality standards (GB 3095–2012) (35 $\mu g/m^3$) and less than 20,000 people living in regions with concentrations lower than 10 $\mu g/m^3$ (World Health Organization (WHO) guideline) in 2017. Regionally, 1% of the Northeast population was exposed to $PM_{2.5}$ concentrations exceeding 50 $\mu g/m^3$, compared to 90% of the Centre population. Typical ambient concentrations in the East and West regions range from 20 to 80 $\mu g/m^3$, while a larger percentage of the population in the East (56%) experienced $PM_{2.5}$ concentrations higher than 50 $\mu g/m^3$ than that in the West (36%), although the mean concentrations in the East are slightly lower than those in the West.

3.2. Ground-level particle radius estimation

The atmospheric aerosols over China were dominated by $PM_{2.5}$ particles with radius less than 1.0 μm in 2017. Due to the dearth of large-scale ground-level radius measurements, the estimated particle radius was validated against the available Aerosol Robotic Network (AERONET) columnar radius retrievals provided by eight stations, with R = 0.66 (Fig. 3a). The detailed information for AERONET measurements is provided in the Supplemental Material. Both RMSE and MAE were less than 0.2 μm, enabling diverse particle sizes to be distinguished. A

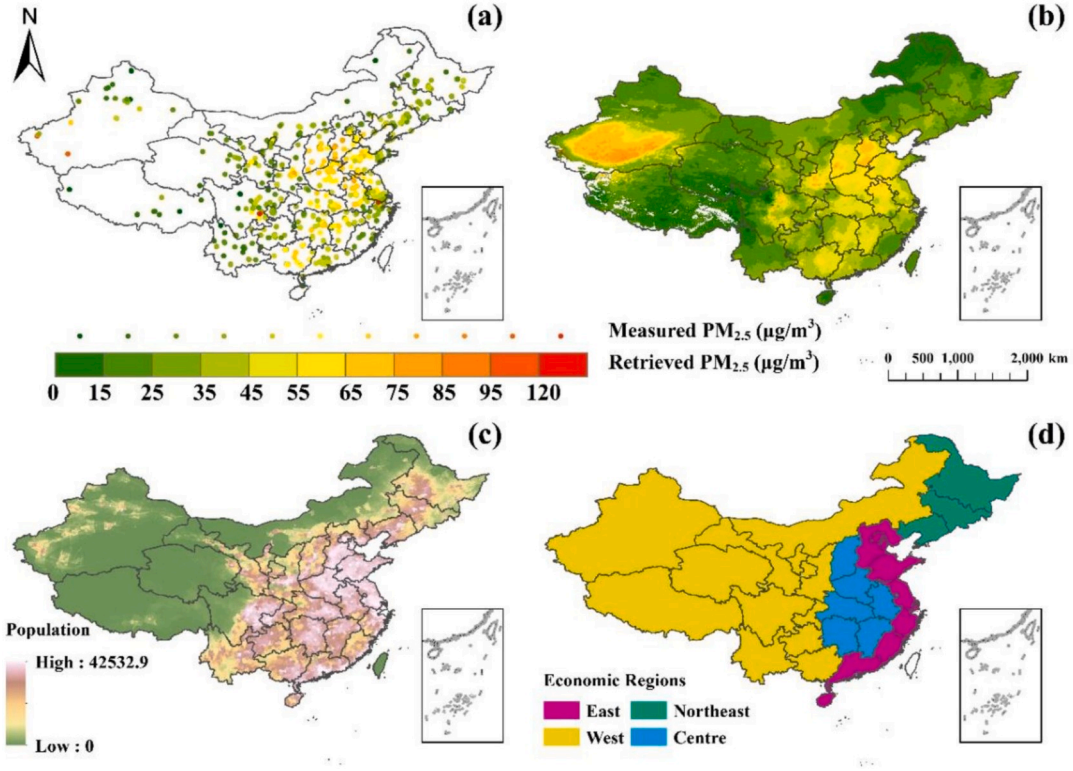

Fig. 1. Spatial patterns of (a) ground-based $PM_{2.5}$ concentrations (b) satellite-estimated $PM_{2.5}$ concentrations (c) population (d) economic regions in 2017 (Note that the following analysis did not take into account Taiwan because of the lack of population data).

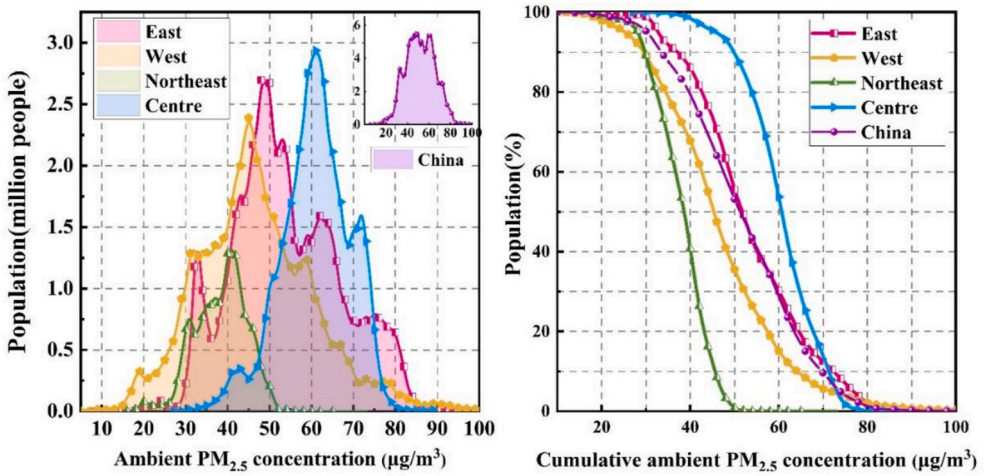

Fig. 2. Distribution of 2017 p.m.$_{2.5}$ concentrations by population for four economic regions and China.

positive MBE indicates that the ground-level estimated radius was slightly larger than the columnar AERONET retrievals, which could be due to a slight decrease in radius with altitude (Baars et al., 2012). We also plotted our radius estimates against the AERONET Angstrom Exponent (AE) values (using wavelengths 0.44 and 0.87 μm) in Fig. 3b. The result shows that the estimated radius decreased with increasing AE and the rate of decline is larger at lower AE values (inset in Fig. 3b). These findings are consistent with previous studies showing that AE is generally inversely associated with particle size (Giannakaki et al., 2016; Müller et al., 2011; Schuster et al., 2006).

Given that limited radius samples cannot fully reveal the nationwide spatial distribution, we also visually compared our estimates to MODIS AE products for each season. The spatial patterns of estimated particle radius are shown for annual and seasonal scales in Fig. 4. The mean particle size is larger in the West than in the Centre or East. The division coincides with the imaginary line (Heihe-Tengchong) dividing the territory of China into western and eastern parts according to population density (Hu, 1935). This result indicates that the population in eastern China is exposed to $PM_{2.5}$ pollution with a smaller mean particle size. This can also be supported by the national patterns of decadal mean mass concentrations of PM_1 and $PM_{2.5}$ from two studies (Chen et al., 2018a; Ma et al., 2016) (details in Supplementary Material). The Tarim Basin (where the Taklamakan Desert is located) has the largest particle size in China, especially in the spring and summer. $PM_{2.5}$ with smaller particle size are more likely to occur in the spring and summer in eastern China, while there is less spatial variation in autumn and winter. The seasonal variations and spatial patterns of the estimated particle radius are visually consistent with those of MODIS AE data.

Fig. 5 presents the distribution of annual-mean particle effective radius by population and region. Nationally, more than 99% of the Chinese population lived in areas with effective particle radius less than 0.7 μm (i.e. aerodynamic diameters lower than 1.0 μm under the assumptions in this study) in 2017. The PWA effective radius of $PM_{2.5}$ in China was estimated to be 0.5 μm, with STD of 0.5 μm (Supplementary Material). This national mean of Re = 0.5 μm was used to compare exposures across the different regions. Fig. 5 shows that 98% of the Centre's population was exposed to particles with annual-mean radius below 0.5 μm, compared to 85% of the Northeast. The Centre was consistently exposed to small particles, with PWA radius of 0.4 μm. Although Fig. 4 shows the West had the largest particles, Fig. 5 shows that most of its population was exposed to relatively smaller ones, with PWA radius of 0.5 μm (rounded to the nearest tenth of a micron).

The seasonality of particle size can be observed in Fig. 6. The biggest difference in the median radius between the four regions occurred in springtime. Half of the Centre population in spring was exposed to $PM_{2.5}$ with radius less than 0.4 μm, while half of the Northeast population was exposed to larger particles, with median radius of 0.5 μm. Only 1% of the Centre population was exposed to particles larger than 0.5 μm in the spring, compared to 84% of the Northeast. Summer is the season with the highest national exposures (86%) to a mean radius less than 0.5 μm. The West shows the least seasonal variation in exposures to a mean less than 0.5 μm (76%–81%). A relatively large proportion of the East

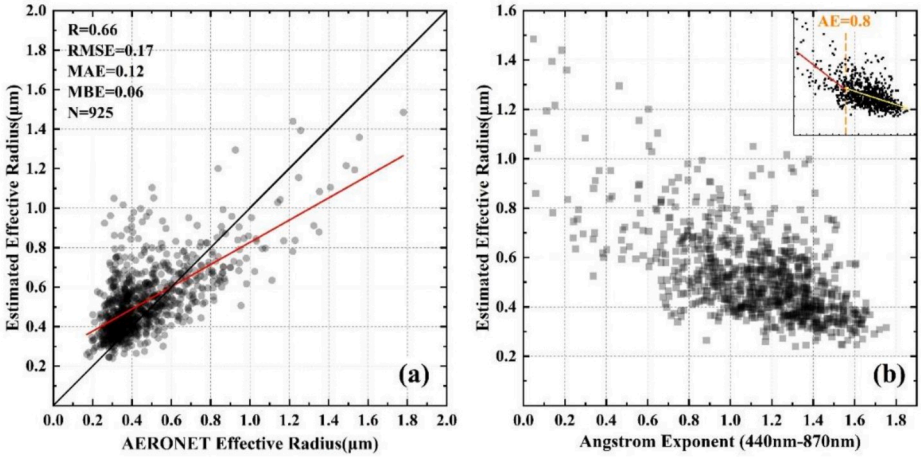

Fig. 3. Validation of estimated effective radius against AERONET (a) radius retrievals and (b) AE values.

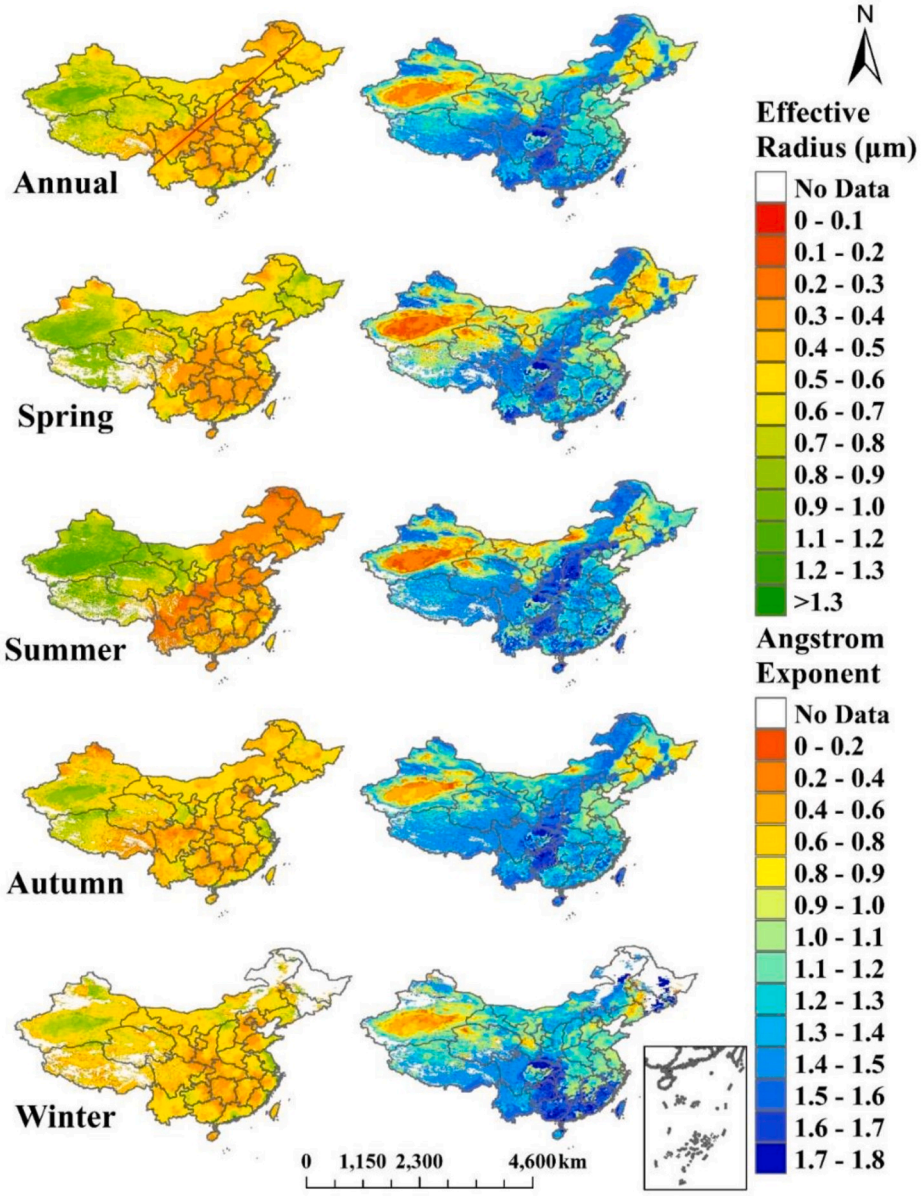

Fig. 4. Spatial patterns of estimated particle effective radius (left) and MODIS Angstrom Exponent (right).

population (42% in autumn and 40% in winter) are exposed to $PM_{2.5}$ (Re > 0.5 μm), likely due to high population density in the coastal region. The results suggest that population in the Centre region was exposed to not only the highest $PM_{2.5}$ concentration but also the smallest particle size.

4. Discussion

Previous studies have shown the potential for particle size to affect outcomes of PM exposure, indicating that smaller sizes may have greater effects on human health (De Haar et al., 2006; Franck et al., 2011). Size-resolved exposures needed to support epidemiologic studies into this effect, however, are limited by a lack of observations, especially at population scales. Here, we quantified $PM_{2.5}$ concentrations using a GWR model and estimated effective particle radius based on optical-mass theoretical relationships for China in 2017 across regions and seasons.

The national, annual-mean $PM_{2.5}$ mass concentration was estimated to be 45.9 μg/m^3. The highest mass concentrations of $PM_{2.5}$ were observed in central and eastern China (east of Heihe-Tengchong population line). These high concentrations were most prevalent in industrialized urban agglomerations, such as the North China Plain (the BTH region), Hubei and Hunan provinces. Higher concentrations were also found to cross into Shanxi and Shaanxi province, areas with abundant coal-fired facilities and coal production. This is consistent with previous attribution studies suggesting that the high $PM_{2.5}$ concentration in these regions is attributable to anthropogenic activities associated with rapid economic development and industrialization, such as fossil fuel consumption (Zhang et al., 2015, 2013; Zheng et al., 2015). The hotspot in the Sichuan Basin is related to the unfavorable topography encouraging stagnation in this low-lying area surrounded by mountains (You et al., 2016).

In the fine fraction ($PM_{2.5}$), we observed a range of annual mean effective particle radii from 0.3 μm to 1.8 μm across China in 2017. On a national, annual scale, we found a mean particle effective radius of 0.5 μm with a STD of 0.5 μm. This is consistent with Wichmann et al. (2000), finding that 78% (14%) of $PM_{2.5}$ mass was found in the diameter range of 0.1–0.5 μm (0.5–1.0 μm) in an urban area in Germany. The largest

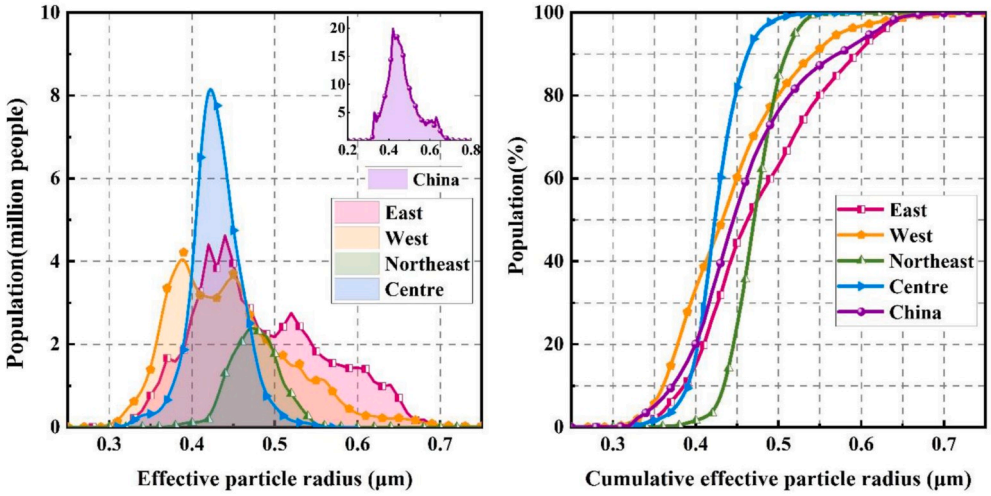

Fig. 5. Distribution of annual-mean $PM_{2.5}$ effective radius estimation for four economic regions and China.

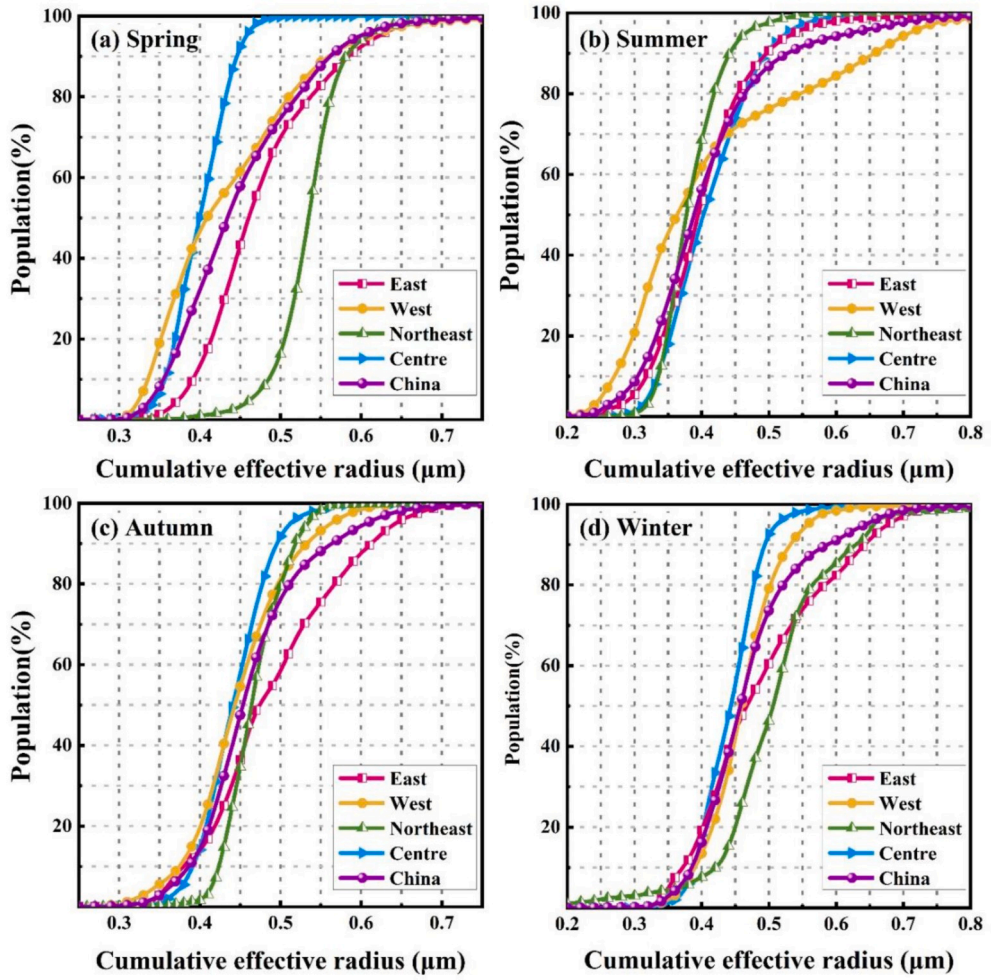

Fig. 6. Distribution of seasonal-mean $PM_{2.5}$ effective radius estimation for four economic regions and China in (a) Spring (b) Summer (c) Autumn and (d) Winter.

mean effective radii of $PM_{2.5}$ were found in the West, which is consistent with the evidence that the contribution of dust-related emission to $PM_{2.5}$ in the West is much higher than other regions (He et al., 2017; Huang et al., 2014). Mean particle radius across the Tarim Basin was much larger than in other areas, ranging from 0.6 μm to 1.4 μm. This finding is expected given the dust and sand in the Taklamakan Desert, and is in line with studies of $PM_{2.5}$ mass and size in this region (Ma et al., 2014; Shao and Mao, 2016). Combining the seasonal spatial patterns of AOD and particle size (Supplementary Material), we found that high values of both AOD particle radius over the Taklamakan Desert are more prevalent in spring, which is attributed to the frequent dust events during spring (Yu et al., 2015; Zhao, 2003). It is interesting to note that large

size values were also observed in summer here. This appears to be supported by Meng et al. (2019), reporting that summer has the lowest ratios of $PM_{2.5}/PM_{10}$, PM_1/PM_{10}, and $PM_1/PM_{2.5}$. Due to a dearth of studies of seasonal patterns of $PM_{2.5}$ composition in this region, however, we can only infer that this observed seasonality could be related to the sources, fate and transport of $PM_{2.5}$, and potential seasonal bias in the input data. Additionally, the Northeast region also experienced relatively high $PM_{2.5}$ concentrations with large particle radii in spring, which has been related to sand and dust storms caused by Siberian and Mongolian cyclones from northern Asia, indicating that the spatial pattern of $PM_{2.5}$ concentrations was also affected by aerosol regional transport (Qian et al., 2004; Wang et al., 2011). The drivers of fine aerosol sizes, such as emissions and meteorological factors, should be explored further to test these inferences. Intraregional analysis was not included in this study since observed differences were mostly small compared to errors.

5. Sources of uncertainty

This study attempts to utilize large-scale measurements to explore the spatial variation and population exposure to ambient size-resolved $PM_{2.5}$ exposure. Given the aims of this work, several assumptions have been proposed to simplify the estimation method. Following error propagation theory, the uncertainty related to assumptions is approximately 24%. Specifically, the assumption that spherical aerosols were uniformly distributed in the PBL can introduce an error of 16% in aerosol extinction, especially when additional pollution layers above the PBL are present due to emissions and long-distance transport of air pollutants (Li et al., 2016). While we assumed that the physiochemical and optical properties of aerosols are independent of size distribution, which enabled the aerosol hygroscopic properties to be simplified by growth functions, previous studies reported minor errors from this assumption (Li et al., 2016; Zieger et al., 2014). In addition to the above theoretical assumptions, empirical assumptions (such as σ_g and ρ) can also bring errors. Two aerosol properties in size estimation were assumed constant, including ρ and σ_g used to define the lognormal distribution. According to previous studies (Hand and Kreidenweis, 2002; Hänel and Thudium, 1977; McMurry et al., 2002), the general range of mass density is 1.5–2.1 g/cm^3 in different regions, therefore, the assumption (ρ = 1.5 g/cm^3) can cause an error of about 16.7% (versus the average density of 1.80 g/cm^3 at multiple sites). The average value of σ_g in the OPAC database for most fine aerosol components is 2.14 μm (Hess et al., 1998), and the constant value of σ_g (2 μm) produces a systematic error of 6% against the average value. The maximum bias (0.01) caused by the constant (3.912) in Koschmieder's equation in extinction when V = 0.2 km. The sensitivity analysis is provided in Supplementary Material.

In addition to assumptions, errors in input data affect the accuracy of the concentration and size estimates. Although MODIS AOD has been widely adopted and validated for daily $PM_{2.5}$ concentration retrieval, biases remain because of the algorithm assumptions and cloud contamination. Missing AOD values may arise due to cloud contamination, leading to underestimation, particular during severe haze. AOD values may also be biased in coastal regions where surface reflectance is more likely to be affected by mixed-pixels and challenging to characterize (Anderson et al., 2013). The validation of MODIS AOD in this study is shown in Fig. S3, with R = 0.92 and RMSE = 0.18. Combining multiple sensors can be an effective way to improve the completeness and accuracy of AOD estimates in the future (Guo et al., 2014; Qi et al., 2013). Other input parameters, for example, from meteorological reanalysis, can also introduce uncertainty due to model assumptions, coarse resolution and interpolation algorithm. Though the quantitative uncertainty of these parameters was not evaluated in this study due to the dearth of measurements, the good performance of reanalysis dataset has been demonstrated in numerous studies (Deroubaix et al., 2019; Ding et al., 2004; Kalnay et al., 1996). Further, errors in $PM_{2.5}$ concentrations (RMSE = 15.7 μg/m^3, MAE = 10.1 μg/m^3) can propagate to particle size estimates; therefore, as $PM_{2.5}$ estimates improve, so too will the reliability of size estimation results.

Differences in spatial and temporal representativeness between satellite observations and ground-level measurements can also impact the estimation results. The satellite data employed in this study represent an average value for a 3 km by 3 km pixel, while monitoring stations represent some area around their sites, which are usually located in highly populated regions. Some temporal inconsistency also persists, given differing measurement frequencies and averaging periods between the ground-based and satellite-based observations.

Compared to a laboratory setting, estimating particle radius accurately using satellite data is difficult due to the characteristics of remote sensing (such as coarse resolution and long-distance measurements). Validation is also a challenge because of the limited ground-based measured data. Though various measurement campaigns have explored particle distributions in China (Song et al., 2012; Tao et al., 2019; Yi et al., 2006), and many studies measured and estimated PM concentrations for different size ranges (including PM_1, $PM_{2.5}$ and PM_{10}) (Shao et al., 2018; Wang et al., 2015; Zang et al., 2019) over specific times and locations, they are difficult to compare to our national, annual average values due to their disparate spatiotemporal scales. This is why we examined the relationship between estimated particle radius, AERONET columnar retrieved radius, and AE data from AERONET and MODIS. As expected, a decreasing pattern between effective radius and AE was observed. While promising, this interpretation is qualitative, as the relationship between AE and particle effective radius is known to vary with wavelength, size distribution, and composition (Gobbi et al., 2007; Schuster et al., 2006). The observed range of mean effective particle radii, 0.3 μm–1.8 μm, is based on an annual average of a single year, and thus cannot fully represent the actual $PM_{2.5}$ size range that may be experienced over time across China. More highly-resolved data with shorter averaging periods over long timescales may reveal a wider range of exposures.

6. Conclusion

This study presents the first, to our knowledge, national estimates of size-resolved exposures to fine particulate matter. It seeks to address a gap in population-scale estimates that could be used to motivate or inform our understanding of the effect of particle size on human health, which current evidence suggests is important but remains limited by data. In an effort to address this gap, we derive particle effective radius and mass concentration of $PM_{2.5}$ using satellite-derived data and aerosol microphysical properties to explore the spatial pattern and population exposure of $PM_{2.5}$ concentrations and sizes.

We find that most of the Chinese population was exposed to high $PM_{2.5}$ concentrations with small particle sizes. Fewer than 20,000 people in 2017 lived in locations where concentrations met the annual WHO guideline (10 μg/m^3). Less than 1% lived in regions with a $PM_{2.5}$ mean particle effective radius above 0.7 μm (i.e. aerodynamic diameters lower than 1.0 μm) in 2017. The national population-weighted annual average concentration of $PM_{2.5}$ and particle effective radius were estimated to be 52.1 μg/m^3 and 0.5 μm in 2017, respectively. Spatially, $PM_{2.5}$ concentrations to the east of the Heihe-Tengchong population line were generally higher than those in the west, while the particle radius was larger in the west, especially in the desert. Specifically, among four economic regions, the Centre region had the highest ambient $PM_{2.5}$ concentrations with the smallest particle radius, where 90% of the population was exposed to $PM_{2.5}$ concentrations higher than 50 μg/m^3 and only 2% was exposed to a mean effective particle radius larger than 0.5 μm in 2017. High $PM_{2.5}$ concentrations and small particle sizes were more likely to occur in regions with high GDP and population densities, which is in line with other work suggesting an important contribution from industrial and economic activity. Temporally, summer is the

season in which the highest percentage of the national population (86%) lived in areas with a mean effective radius of $PM_{2.5}$ less than 0.5 μm. In the Taklamakan Desert, where aerosols are dominated by natural sources (such as dust and sand), large particle radii were more prevalent in spring due to the higher frequency of dust events, despite relatively low $PM_{2.5}$ concentrations during this period.

The validation of particle radius in this work is restricted by the available particle size measurements. Large-scale and long-term particle size measurements in polluted regions, such as India and China, are especially limited. The AERONET columnar radius retrievals and MODIS AE data provide large-coverage observations of a variable linked to aerosol size were used to validate our radius estimates, yielding an MAE of 0.12 μm. Sensitivity analysis of retrieval parameters found a potential MAE contribution of 0.1 μm. Some of this difference may be attributable to differences in retrieval approaches. Accuracy may be improved with the advent of further ground-based measurements, higher resolution data input, or more detailed information on aerosol properties. This work demonstrates the potential of remote sensing techniques for estimating population-scale size-resolved $PM_{2.5}$ exposures, reveals prevalent exposure to sub-micron particles, and motivates further research on the effect of particle size on health outcomes related to particulate matter.

Declaration of competing interest

The authors declare that they have no known competing financial interests or personal relationships that could have appeared to influence the work reported in this paper.

CRediT authorship contribution statement

Ming Liu: Conceptualization, Methodology, Software, Investigation, Writing - original draft. **Rebecca K. Saari:** Supervision, Conceptualization, Writing - review & editing. **Gaoxiang Zhou:** Software, Investigation. **Xiangnan Liu:** Writing - review & editing. **Jonathan Li:** Supervision, Writing - review & editing.

Acknowledgements

The first author acknowledges the China Scholarship Council for their support via a doctoral scholarship (No. 201706400072). Rebecca K. Saari acknowledges funding by the Natural Sciences and Engineering Research Council of Canada.

Appendix A. Supplementary data

Supplementary data to this article can be found online at https://doi.org/10.1016/j.atmosenv.2020.117745.

References

Anderson, J.C., Wang, J., Zeng, J., Leptoukh, G., Petrenko, M., Ichoku, C., Hu, C., 2013. Long-term statistical assessment of Aqua-MODIS aerosol optical depth over coastal regions: bias characteristics and uncertainty sources. Tellus B 65, 20805. https://doi.org/10.3402/tellusb.v65i0.20805.

Baars, H., Ansmann, A., Althausen, D., Engelmann, R., Heese, B., Müller, D., Artaxo, P., Paixao, M., Pauliquevis, T., Souza, R., 2012. Aerosol profiling with lidar in the Amazon Basin during the wet and dry season. J. Geophys. Res. Atmospheres 117. https://doi.org/10.1029/2012JD018338.

Brauer, M., Amann, M., Burnett, R.T., Cohen, A., Dentener, F., Ezzati, M., Henderson, S. B., Krzyzanowski, M., Martin, R.V., Van Dingenen, R., van Donkelaar, A., Thurston, G.D., 2012. Exposure assessment for estimation of the global burden of disease attributable to outdoor air pollution. Environ. Sci. Technol. 46, 652–660. https://doi.org/10.1021/es2025752.

Chen, G., Knibbs, L.D., Zhang, W., Li, S., Cao, W., Guo, J., Ren, H., Wang, B., Wang, H., Williams, G., Hamm, N.A.S., Guo, Y., 2018a. Estimating spatiotemporal distribution of PM1 concentrations in China with satellite remote sensing, meteorology, and land use information. Environ. Pollut. 233, 1086–1094. https://doi.org/10.1016/j.envpol.2017.10.011.

Chen, G., Li, S., Zhang, Y., Zhang, W., Li, D., Wei, X., He, Y., Bell, M.L., Williams, G., Marks, G.B., Jalaludin, B., Abramson, M.J., Guo, Y., 2017. Effects of ambient PM1 air pollution on daily emergency hospital visits in China: an epidemiological study. Lancet Planet. Health 1, e221–e229. https://doi.org/10.1016/S2542-5196(17)30100-6.

Chen, G., Morawska, L., Zhang, W., Li, S., Cao, W., Ren, H., Wang, B., Wang, H., Knibbs, L.D., Williams, G., Guo, J., Guo, Y., 2018b. Spatiotemporal variation of PM1 pollution in China. Atmos. Environ. 178, 198–205. https://doi.org/10.1016/j.atmosenv.2018.01.053.

Chen, J., Zhao, C.S., Ma, N., Yan, P., 2014. Aerosol hygroscopicity parameter derived from the light scattering enhancement factor measurements in the North China Plain. Atmos. Chem. Phys. 14, 8105–8118. https://doi.org/10.5194/acp-14-8105-2014.

Chen, Y., Zhao, P., He, D., Dong, F., Zhao, X., Zhang, X., 2015. Characteristics and parameterization for atmospheric extinction coefficient in beijing. Environ. Sci. 36, 3582–3589.

Clarisse, L., Hurtmans, D., Prata, A.J., Karagulian, F., Clerbaux, C., Mazière, M.D., Coheur, P.-F., 2010. Retrieving radius, concentration, optical depth, and mass of different types of aerosols from high-resolution infrared nadir spectra. Appl. Optic. 49, 3713–3722. https://doi.org/10.1364/AO.49.003713.

Cohen, A.J., Brauer, M., Burnett, R., Anderson, H.R., Frostad, J., Estep, K., Balakrishnan, K., Brunekreef, B., Dandona, L., Dandona, R., Feigin, V., Freedman, G., Hubbell, B., Jobling, A., Kan, H., Knibbs, L., Liu, Y., Martin, R., Morawska, L., Pope 3rd, C.A., Shin, H., Straif, K., Shaddick, G., Thomas, M., van Dingenen, R., van Donkelaar, A., Vos, T., Murray, C.J.L., Forouzanfar, M.H., 2017. Estimates and 25-year trends of the global burden of disease attributable to ambient air pollution: an analysis of data from the Global Burden of Diseases Study 2015. Lancet 389, 1907–1918. https://doi.org/10.1016/S0140-6736(17)30505-6.

Day, M.C., Pandis, S.N., 2011. Predicted changes in summertime organic aerosol concentrations due to increased temperatures. Atmos. Environ. 45, 6546–6556. https://doi.org/10.1016/j.atmosenv.2011.08.028.

De Haar, C., Hassing, I., Bol, M., Bleumink, R., Pieters, R., 2006. Ultrafine but not fine particulate matter causes airway inflammation and allergic airway sensitization to co-administered antigen in mice. Clin. Exp. Allergy 36, 1469–1479.

Delfino, R.J., Sioutas, C., Malik, S., 2005. Potential role of ultrafine particles in associations between airborne particle mass and cardiovascular health. Environ. Health Perspect. 113, 934–946. https://doi.org/10.1289/ehp.7938.

Deroubaix, A., Menut, L., Flamant, C., Brito, J., Denjean, C., Dreiling, V., Fink, A., Jambert, C., Kalthoff, N., Knippertz, P., Ladkin, R., Mailler, S., Maranan, M., Pacifico, F., Piguet, B., Siour, G., Turquety, S., 2019. Diurnal cycle of coastal anthropogenic pollutant transport over southern West Africa during the DACCIWA campaign. Atmos. Chem. Phys. 19, 473–497. https://doi.org/10.5194/acp-19-473-2019.

Ding, A., Wang, Tao, Zhao, M., Wang, Tijian, Li, Z., 2004. Simulation of sea-land breezes and a discussion of their implications on the transport of air pollution during a multi-day ozone episode in the Pearl River Delta of China. Atmos. Environ. 38, 6737–6750. https://doi.org/10.1016/j.atmosenv.2004.09.017.

Esposito, V., Lucariello, A., Savarese, L., Cinelli, M.P., Ferraraccio, F., Bianco, A., De Luca, A., Mazzarella, G., 2012. Morphology changes in human lung epithelial cells after exposure to diesel exhaust micron sub particles (PM1.0) and pollen allergens. Environ. Pollut. 171, 162–167. https://doi.org/10.1016/j.envpol.2012.07.006.

Franck, U., Odeh, S., Wiedensohler, A., Wehner, B., Herbarth, O., 2011. The effect of particle size on cardiovascular disorders — the smaller the worse. Sci. Total Environ. 409, 4217–4221. https://doi.org/10.1016/j.scitotenv.2011.05.049.

Gerlofs-Nijland, M.E., Rummelhard, M., Boere, A.J.F., Leseman, D.L.A.C., Duffin, R., Schins, R.P.F., Borm, P.J.A., Sillanpää, M., Salonen, R.O., Cassee, R.F., 2009. Particle induced toxicity in relation to transition metal and polycyclic aromatic hydrocarbon contents. Environ. Sci. Technol. 43, 4729–4736. https://doi.org/10.1021/es803176k.

Giannakaki, E., van Zyl, P.G., Müller, D., Balis, D., Komppula, M., 2016. Optical and microphysical characterization of aerosol layers over South Africa by means of multi-wavelength depolarization and Raman lidar measurements. Atmos. Chem. Phys. 16, 8109–8123. https://doi.org/10.5194/acp-16-8109-2016.

Gobbi, G.P., Kaufman, Y.J., Koren, I., Eck, T.F., 2007. Classification of aerosol properties derived from AERONET direct sun data. Atmos. Chem. Phys. 7, 453–458. https://doi.org/10.5194/acp-7-453-2007.

Gulliver, J., Briggs, D.J., 2007. Journey-time exposure to particulate air pollution. Atmos. Environ. 41, 7195–7207. https://doi.org/10.1016/j.atmosenv.2007.05.023.

Guo, J., Gu, X., Yu, T., Cheng, T., Chen, H., 2014. Trend analysis of the aerosol optical depth from fusion of MISR and MODIS retrievals over China. IOP Conf. Ser. Earth Environ. Sci. 17 https://doi.org/10.1088/1755-1315/17/1/012036, 012036.

Hand, J.L., Kreidenweis, S.M., 2002. A new method for retrieving particle refractive index and effective density from aerosol size distribution data. Aerosol. Sci. Technol. 36, 1012–1026. https://doi.org/10.1080/02786820290092276.

Hänel, G., Thudium, J., 1977. Mean bulk densities of samples of dry atmospheric aerosol particles: A summary of measured data. PAGEOPH 115, 799–803. https://doi.org/10.1007/BF00881211.

He, J., Gong, S., Yu, Y., Yu, L., Wu, L., Mao, H., Song, C., Zhao, S., Liu, H., Li, X., Li, R., 2017. Air pollution characteristics and their relation to meteorological conditions during 2014–2015 in major Chinese cities. Environ. Pollut. 223, 484–496. https://doi.org/10.1016/j.envpol.2017.01.050.

He, Q., Huang, B., 2018. Satellite-based mapping of daily high-resolution ground PM2.5 in China via space-time regression modeling. Remote Sens. Environ. 206, 72–83. https://doi.org/10.1016/j.rse.2017.12.018.

Hess, M., Koepke, P., Schult, I., 1998. Optical properties of aerosols and clouds: The software package OPAC. Bull. Am. Meteorol. Soc. 79, 831–844.

Hilboll, A., Richter, A., Burrows, J.P., 2013. Long-term changes of tropospheric NO2 over megacities derived from multiple satellite instruments. Atmos. Chem. Phys. 13, 4145–4169. https://doi.org/10.5194/acp-13-4145-2013.

Hoek, G., Boogaard, H., Knol, A., De Hartog, J., Slottje, P., Ayres, J.G., Borm, P., Brunekreef, B., Donaldson, K., Forastiere, F., 2009. Concentration response functions for ultrafine particles and all-cause mortality and hospital admissions: results of a European expert panel elicitation. Environ. Sci. Technol. 44, 476–482.

Holben, B.N., Eck, T.F., Slutsker, I., Tanré, D., Buis, J.P., Setzer, A., Vermote, E., Reagan, J.A., Kaufman, Y.J., Nakajima, T., Lavenu, F., Jankowiak, I., Smirnov, A., 1998. AERONET—a federated instrument network and data archive for aerosol characterization. Remote Sens. Environ. 66, 1–16. https://doi.org/10.1016/S0034-4257(98)00031-5.

Hu, H.Y., 1935. The distribution of population in China,with Statistics and maps. Acta Geograph. Sin. 2, 33–74. https://doi.org/10.11821/xb193502002.

Hu, K., Guo, Y., Hu, D., Du, R., Yang, X., Zhong, J., Fei, F., Chen, F., Chen, G., Zhao, Q., Yang, J., Zhang, Y., Chen, Q., Ye, T., Li, S., Qi, J., 2018. Mortality burden attributable to PM1 in Zhejiang province, China. Environ. Int. 121, 515–522. https://doi.org/10.1016/j.envint.2018.09.033.

Huang, R.-J., Zhang, Y., Bozzetti, C., Ho, K.-F., Cao, J.-J., Han, Y., Daellenbach, K.R., Slowik, J.G., Platt, S.M., Canonaco, F., Zotter, P., Wolf, R., Pieber, S.M., Bruns, E.A., Crippa, M., Ciarelli, G., Piazzalunga, A., Schwikowski, M., Abbaszade, G., Schnelle-Kreis, J., Zimmermann, R., An, Z., Szidat, S., Baltensperger, U., Haddad, I.E., Prévôt, A.S.H., 2014. High secondary aerosol contribution to particulate pollution during haze events in China. Nature 514, 218–222. https://doi.org/10.1038/nature13774.

Kalnay, E., Kanamitsu, M., Kistler, R., Collins, W., Deaven, D., Gandin, L., Iredell, M., Saha, S., White, G., Woollen, J., Zhu, Y., Chelliah, M., Ebisuzaki, W., Higgins, W., Janowiak, J., Mo, K.C., Ropelewski, C., Wang, J., Leetmaa, A., Reynolds, R., Jenne, R., Joseph, D., 1996. The NCEP/NCAR 40-year reanalysis project. Bull. Am. Meteorol. Soc. 77, 437–472. https://doi.org/10.1175/1520-0477(1996)077<0437:TNYRP>2.0.CO;2.

Kaufman, Y.J., Haywood, J.M., Hobbs, P.V., Hart, W., Kleidman, R., Schmid, B., 2003. Remote sensing of vertical distributions of smoke aerosol off the coast of Africa. Geophys. Res. Lett. 30 https://doi.org/10.1029/2003GL017068.

Kloog, I., Nordio, F., Coull, B.A., Schwartz, J., 2012. Incorporating local land use regression and satellite aerosol optical depth in a hybrid model of spatiotemporal PM2.5 exposures in the Mid-Atlantic States. Environ. Sci. Technol. 46, 11913–11921. https://doi.org/10.1021/es302673e.

Knibbs, L.D., van Donkelaar, A., Martin, R.V., Bechle, M.J., Brauer, M., Cohen, D.D., Cowie, C.T., Dirgawati, M., Guo, Y., Hanigan, I.C., Johnston, F.H., Marks, G.B., Marshall, J.D., Pereira, G., Jalaludin, B., Heyworth, J.S., Morgan, G.G., Barnett, A.G., 2018. Satellite-based land-use regression for continental-scale long-term ambient PM2.5 exposure assessment in Australia. Environ. Sci. Technol. 52, 12445–12455. https://doi.org/10.1021/acs.est.8b02328.

Kodros, J.K., Cucinotta, R., Ridley, D.A., Wiedinmyer, C., Pierce, J.R., 2016. The aerosol radiative effects of uncontrolled combustion of domestic waste. Atmos. Chem. Phys. 16, 6771–6784. https://doi.org/10.5194/acp-16-6771-2016.

Kodros, J.K., Pierce, J.R., 2017. Important global and regional differences in aerosol cloud-albedo effect estimates between simulations with and without prognostic aerosol microphysics. J. Geophys. Res. Atmospheres 122, 4003–4018. https://doi.org/10.1002/2016JD025886.

Kodros, J.K., Volckens, J., Jathar, S.H., Pierce, J.R., 2018. Ambient particulate matter size distributions drive regional and global variability in particle deposition in the respiratory tract. Geohealth 2, 298–312. https://doi.org/10.1029/2018gh000145.

Koschmieder, H., 1924. Theorie der horizontalen sichtweite. Beitrage Zur Phys. Freien Atmosphare 33–53.

Kumar, P., Morawska, L., Martani, C., Biskos, G., Neophytou, M., Di Sabatino, S., Bell, M., Norford, L., Britter, R., 2015. The rise of low-cost sensing for managing air pollution in cities. Environ. Int. 75, 199–205. https://doi.org/10.1016/j.envint.2014.11.019.

Larkin, A., Geddes, J.A., Martin, R.V., Xiao, Q., Liu, Y., Marshall, J.D., Brauer, M., Hystad, P., 2017. Global land use regression model for nitrogen dioxide air pollution. Environ. Sci. Technol. 51, 6957–6964. https://doi.org/10.1021/acs.est.7b01148.

Li, Z.Q., Zhang, Y., Shao, J., Li, B.S., Hong, J., Liu, D., Li, D.H., Wei, P., Li, W., Li, L., Zhang, F.X., Guo, J., Deng, Q., Wang, B.X., Cui, C.L., Zhang, W.C., Wang, Z.Z., Lv, Y., Xu, H., Chen, X.F., Li, L., Qie, L.L., 2016. Remote sensing of atmospheric particulate mass of dry PM2.5 near the ground: method validation using ground-based measurements. Remote Sens. Environ. 173, 59–68. https://doi.org/10.1016/j.rse.2015.11.019.

Lin, H., Tao, J., Du, Y., Liu, T., Qian, Z., Tian, L., Di, Q., Rutherford, S., Guo, L., Zeng, W., Xiao, J., Li, X., He, Z., Xu, Y., Ma, W., 2016. Particle size and chemical constituents of ambient particulate pollution associated with cardiovascular mortality in Guangzhou, China. Environ. Pollut. 208, 758–766. https://doi.org/10.1016/j.envpol.2015.10.056.

Liu, Y., Franklin, M., Kahn, R., Koutrakis, P., 2007. Using aerosol optical thickness to predict ground-level PM2.5 concentrations in the St. Louis area: A comparison between MISR and MODIS. Remote Sensing of Environment, Multi-angle Imaging Spectro Radiometer (MISR) 107, 33–44. https://doi.org/10.1016/j.rse.2006.05.022. Special Issue.

Liu, Y., Paciorek, C.J., Koutrakis, P., 2009. Estimating regional spatial and temporal variability of PM2.5 concentrations using satellite data, meteorology, and land use information. Environ. Health Perspect. 117, 886–892. https://doi.org/10.1289/ehp.0800123.

Liu, M., Zhou, G., Saari, R.K., Li, J., 2019a. Long-term trend of ground-level PM2.5 concentrations over 2012-2017 in China. In: IGARSS 2019 - 2019 IEEE International Geoscience and Remote Sensing Symposium. Presented at the IGARSS 2019 - 2019 IEEE International Geoscience and Remote Sensing Symposium. IEEE, Yokohama, Japan, pp. 7842–7845. https://doi.org/10.1109/IGARSS.2019.8900405.

Liu, M., Zhou, G., Saari, R.K., Li, S., Liu, X., Li, J., 2019b. Quantifying PM2.5 mass concentration and particle radius using satellite data and an optical-mass conversion algorithm. ISPRS J. Photogrammetry Remote Sens. 158, 90–98. https://doi.org/10.1016/j.isprsjprs.2019.10.010.

Ma, Z., Hu, X., Huang, L., Bi, J., Liu, Y., 2014. Estimating ground-level PM2.5 in China using satellite remote sensing. Environ. Sci. Technol. 48, 7436–7444. https://doi.org/10.1021/es5009399.

Ma, Z., Hu, X., Sayer, A.M., Levy, R., Zhang, Q., Xue, Y., Tong, S., Bi, J., Huang, L., Liu, Y., 2016. Satellite-based spatiotemporal trends in PM2.5 concentrations: China, 2004-2013. Environ. Health Perspect. 124, 184–192. https://doi.org/10.1289/ehp.1409481.

McMurry, P.H., Wang, X., Park, K., Ehara, K., 2002. The relationship between mass and mobility for atmospheric particles: a new technique for measuring particle density. Aerosol. Sci. Technol. 36, 227–238. https://doi.org/10.1080/02786820275350408 3.

Meng, X., Wu, Y., Pan, Z., Wang, H., Yin, G., Zhao, H., 2019. Seasonal characteristics and particle-size distributions of particulate air pollutants in urumqi. Int. J. Environ. Res. Publ. Health 16, 396. https://doi.org/10.3390/ijerph16030396.

Mills, N.L., Donaldson, K., Hadoke, P.W., Boon, N.A., MacNee, W., Cassee, F.R., Sandström, T., Blomberg, A., Newby, D.E., 2009. Adverse cardiovascular effects of air pollution. Nat. Clin. Pract. Cardiovasc. Med. 6, 36–44. https://doi.org/10.1038/ncpcardio1399.

Müller, T., Schladitz, A., Kandler, K., Wiedensohler, A., 2011. Spectral particle absorption coefficients, single scattering albedos and imaginary parts of refractive indices from ground based in situ measurements at Cape Verde Island during SAMUM-2. Tellus B 63, 573–588. https://doi.org/10.1111/j.1600-0889.2011.00572.x.

Nakajima, T., Tonna, G., Rao, R., Boi, P., Kaufman, Y., Holben, B., 1996. Use of sky brightness measurements from ground for remote sensing of particulate polydispersions. Appl. Optic. 35, 2672–2686. https://doi.org/10.1364/AO.35.002672.

Ostro, B., Hu, J., Goldberg, D., Reynolds, P., Hertz, A., Bernstein, L., Kleeman, M.J., 2015. Associations of mortality with long-term exposures to fine and ultrafine particles, species and sources: results from the California Teachers Study Cohort. Environ. Health Perspect. 123, 549–556. https://doi.org/10.1289/ehp.1408565.

Pacitto, A., Stabile, L., Moreno, T., Kumar, P., Wierzbicka, A., Morawska, L., Buonanno, G., 2018. The influence of lifestyle on airborne particle surface area doses received by different Western populations. Environ. Pollut. 232, 113–122. https://doi.org/10.1016/j.envpol.2017.09.023.

Pekkanen, J., Kulmala, M., 2004. Exposure assessment of ultrafine particles in epidemiologic time-series studies. Scand. J. Work. Environ. Health 30, 9–18.

Pekkanen, J., Pearce, N., 2001. Environmental epidemiology: challenges and opportunities. Environ. Health Perspect. 109, 1–5. https://doi.org/10.1289/ehp.011091.

Pinto, J.P., Lefohn, A.S., Shadwick, D.S., 2004. Spatial variability of PM2.5 in urban areas in the United States. J. Air Waste Manag. Assoc. 54, 440–449. https://doi.org/10.1080/10473289.2004.10470919.

Pope, C.A., Ezzati, M., Cannon, J.B., Allen, R.T., Jerrett, M., Burnett, R.T., 2018. Mortality risk and PM2.5 air pollution in the USA: an analysis of a national prospective cohort. Air Qual. Atmosphere Health 11, 245–252. https://doi.org/10.1007/s11869-017-0535-3.

Qi, Y.L., Ge, J.M., Huang, J.P., 2013. Spatial and temporal distribution of MODIS and MISR aerosol optical depth over northern China and comparison with AERONET. Chin. Sci. Bull. 58, 2497–2506. https://doi.org/10.1007/s11434-013-5678-5.

Qian, W., Tang, X., Quan, L., 2004. Regional characteristics of dust storms in China. Atmos. Environ. 38, 4895–4907. https://doi.org/10.1016/j.atmosenv.2004.05.038.

Reid, J.S., Jonsson, H.H., Maring, H.B., Smirnov, A., Savoie, D.L., Cliff, S.S., Reid, E.A., Livingston, J.M., Meier, M.M., Dubovik, O., Tsay, S.-C., 2003. Comparison of size and morphological measurements of coarse mode dust particles from Africa. J. Geophys. Res. Atmospheres 108. https://doi.org/10.1029/2002JD002485.

Roberts, D.R., Bahn, V., Ciuti, S., Boyce, M.S., Elith, J., Guillera-Arroita, G., Hauenstein, S., Lahoz-Monfort, J.J., Schröder, B., Thuiller, W., Warton, D.I., Wintle, B.A., Hartig, F., Dormann, C.F., 2017. Cross-validation strategies for data with temporal, spatial, hierarchical, or phylogenetic structure. Ecography 40, 913–929. https://doi.org/10.1111/ecog.02881.

Saari, R.K., Mei, Y., Monier, E., Garcia-Menendez, F., 2019. Effect of health-related uncertainty and natural variability on health impacts and cobenefits of climate policy. Environ. Sci. Technol. 53, 1098–1108. https://doi.org/10.1021/acs.est.8b05094.

Sacks, J.D., Stanek, L.W., Luben, T.J., Johns, D.O., Buckley, B.J., Brown, J.S., Ross, M., 2011. Particulate matter-induced health effects: who is susceptible? Environ. Health Perspect. 119, 446–454. https://doi.org/10.1289/ehp.1002255.

Saha, P.K., Li, H.Z., Apte, J.S., Robinson, A.L., Presto, A.A., 2019. Urban ultrafine particle exposure assessment with land-use regression: influence of sampling strategy. Environ. Sci. Technol. 53, 7326–7336. https://doi.org/10.1021/acs.est.9b02086.

Samoli, E., Andersen, Z.J., Katsouyanni, K., Hennig, F., Kuhlbusch, T.A.J., Bellander, T., Cattani, G., Cyrys, J., Forastiere, F., Jacquemin, B., Kulmala, M., Lanki, T., Loft, S., Massling, A., Tobias, A., Stafoggia, M., Uf&Health Study group, 2016. Exposure to ultrafine particles and respiratory hospitalisations in five European cities. Eur. Respir. J. 48, 674–682. https://doi.org/10.1183/13993003.02108-2015.

Schuster, G.L., Dubovik, O., Holben, B.N., 2006. Angstrom exponent and bimodal aerosol size distributions. J. Geophys. Res. Atmospheres 111. https://doi.org/10.1029/2005JD006328.

Shao, J., Mao, J., 2016. Dust particle size distributions during spring in yinchuan, China. Adv. Meteorol. 8 https://doi.org/10.1155/2016/6940502, 2016.

Shao, P., Tian, H., Sun, Y., Liu, H., Wu, B., Liu, S., Liu, X., Wu, Y., Liang, W., Wang, Y., Gao, J., Xue, Y., Bai, X., Liu, W., Lin, S., Hu, G., 2018. Characterizing remarkable changes of severe haze events and chemical compositions in multi-size airborne particles (PM1, PM2.5 and PM10) from January 2013 to 2016–2017 winter in Beijing, China. Atmos. Environ. 189, 133–144. https://doi.org/10.1016/j.atmosenv.2018.06.038.

Song, S., Wu, Y., Jiang, J., Yang, L., Cheng, Y., Hao, J., 2012. Chemical characteristics of size-resolved PM2.5 at a roadside environment in Beijing, China. Environ. Pollut., Mercury in the Laurentian Great Lakes Region 161, 215–221. https://doi.org/10.1016/j.envpol.2011.10.014.

Steele, H.M., Eldering, A., Lumpe, J.D., 2006. Simulations of the accuracy in retrieving stratospheric aerosol effective radius, composition, and loading from infrared spectral transmission measurements. Appl. Optic. 45, 2014–2027. https://doi.org/10.1364/AO.45.002014.

Tao, J., Zhang, Z., Wu, Y., Zhang, L., Wu, Z., Cheng, P., Li, M., Chen, L., Zhang, R., Cao, J., 2019. Impact of particle number and mass size distributions of major chemical components on particle mass scattering efficiency in urban Guangzhou in southern China. Atmos. Chem. Phys. 19, 8471–8490. https://doi.org/10.5194/acp-19-8471-2019.

van Donkelaar, A., Martin, R.V., Brauer, M., Hsu, N.C., Kahn, R.A., Levy, R.C., Lyapustin, A., Sayer, A.M., Winker, D.M., 2016. Global estimates of fine particulate matter using a combined geophysical-statistical method with information from satellites, models, and monitors. Environ. Sci. Technol. 50, 3762–3772. https://doi.org/10.1021/acs.est.5b05833.

Wang, S., Liu, X., Yang, X., Zou, B., Wang, J., 2018. Spatial variations of PM2.5 in Chinese cities for the joint impacts of human activities and natural conditions: A global and local regression perspective. J. Clean. Prod. 203, 143–152. https://doi.org/10.1016/j.jclepro.2018.08.249.

Wang, H., Zhang, L., Cao, X., Zhang, Z., Liang, J., 2013. A-Train satellite measurements of dust aerosol distributions over northern China. J. Quant. Spectrosc. Radiat. Transf., INTERNATIONAL SYMPOSIUM ON ATMOSPHERIC LIGHT SCATTERING AND REMOTE SENSING (ISALSaRS'11) 122, 170–179. https://doi.org/10.1016/j.jqsrt.2012.08.011.

Wang, Y.Q., Zhang, X.Y., Sun, J.Y., Zhang, X.C., Che, H.Z., Li, Y., 2015. Spatial and temporal variations of the concentrations of PM10, PM2.5 and PM1 in China. Atmos. Chem. Phys. 15, 13585–13598. https://doi.org/10.5194/acp-15-13585-2015.

Wang, X., Zhang, C., Wang, H., Qian, G., Luo, W., Lu, J., Wang, L., 2011. The significance of Gobi desert surfaces for dust emissions in China: an experimental study. Environ. Earth Sci. 64, 1039–1050. https://doi.org/10.1007/s12665-011-0922-2.

Wichmann, H.E., Spix, C., Tuch, T., Wölke, G., Peters, A., Heinrich, J., Kreyling, W.G., Heyder, J., 2000. Daily mortality and fine and ultrafine particles in Erfurt, Germany part I: role of particle number and particle mass. Res. Rep. Health Eff. Inst. 5–86 discussion 87-94.

Xiao, Q., Chang, H.H., Geng, G., Liu, Y., 2018. An ensemble machine-learning model to predict historical PM2.5 concentrations in China from satellite data. Environ. Sci. Technol. 52, 13260–13269. https://doi.org/10.1021/acs.est.8b02917.

Xu, X., 2017. 1 KM grid population dataset of China. https://doi.org/10.12078/2017121101.

Yan, X., Shi, W., Li, Zhanqing, Li, Zhengqiang, Luo, N., Zhao, W., Wang, H., Yu, X., 2017. Satellite-based PM 2.5 estimation using fine-mode aerosol optical thickness over China. Atmos. Environ. 170, 290–302. https://doi.org/10.1016/j.atmosenv.2017.09.023.

Yang, B.-Y., Qian, Z. (Min), Li, S., Fan, S., Chen, G., Syberg, K.M., Xian, H., Wang, S.-Q., Ma, H., Chen, D.-H., Yang, M., Liu, K.-K., Zeng, X.-W., Hu, L.-W., Guo, Y., Dong, G.-H., 2018. Long-term exposure to ambient air pollution (including PM1) and metabolic syndrome: the 33 Communities Chinese Health Study (33CCHS). Environ. Res. 164, 204–211. https://doi.org/10.1016/j.envres.2018.02.029.

Yi, H., Guo, X., Hao, J., Duan, L., Li, X., 2006. Characteristics of inhalable particulate matter concentration and size distribution from power plants in China. J. Air Waste Manag. Assoc. 56, 1243–1251. https://doi.org/10.1080/10473289.2006.10464590.

You, W., Zang, Z., Zhang, L., Li, Y., Pan, X., Wang, W., 2016. National-scale estimates of ground-level PM2.5 concentration in China using geographically weighted regression based on 3 km resolution MODIS AOD. Rem. Sens. 8, 184. https://doi.org/10.3390/rs8030184.

Yu, J., Che, H., Chen, Q., Xia, X., Zhao, H., Wang, H.Y., Wang, Y., Zhang, X.S., Shi, G., 2015. Investigation of aerosol optical depth (AOD) and Ångström exponent over the desert region of northwestern China based on measurements from the China Aerosol Remote Sensing Network (CARSNET). Aerosol Air Qual. Res. 15, 2024–2036. https://doi.org/10.4209/aaqr.2014.12.0326.

Yu, Q., Lu, Y., Xiao, S., Shen, J., Li, X., Ma, W., Chen, L., 2012. Commuters' exposure to PM1 by common travel modes in Shanghai. Atmos. Environ. Times 59, 39–46. https://doi.org/10.1016/j.atmosenv.2012.06.001.

Zhang, L., Liu, L., Zhao, Y., Gong, S., Zhang, X., Henze, D.K., Capps, S.L., Fu, T.-M., Zhang, Q., Wang, Y., 2015. Source attribution of particulate matter pollution over North China with the adjoint method. Environ. Res. Lett. 10 https://doi.org/10.1088/1748-9326/10/8/084011, 084011.

Zang, L., Mao, F., Guo, J., Wang, W., Pan, Z., Shen, H., Zhu, B., Wang, Z., 2019. Estimation of spatiotemporal PM1.0 distributions in China by combining PM2.5 observations with satellite aerosol optical depth. Sci. Total Environ. 658, 1256–1264. https://doi.org/10.1016/j.scitotenv.2018.12.297.

Zhang, R., Jing, J., Tao, J., Hsu, S.-C., Wang, G., Cao, J., Lee, C.S.L., Zhu, L., Chen, Z., Zhao, Y., Shen, Z., 2013. Chemical characterization and source apportionment of $PM_{2.5}$ in Beijing: seasonal perspective. Atmos. Chem. Phys. 13, 7053–7074. https://doi.org/10.5194/acp-13-7053-2013.

Zhang, Y., Li, Z., 2015. Remote sensing of atmospheric fine particulate matter (PM2.5) mass concentration near the ground from satellite observation. Remote Sens. Environ. 160, 252–262. https://doi.org/10.1016/j.rse.2015.02.005.

Zhao, T.L., 2003. Modeled size-segregated wet and dry deposition budgets of soil dust aerosol during ACE-Asia 2001: implications for trans-Pacific transport. J. Geophys. Res. 108, 8665. https://doi.org/10.1029/2002JD003363.

Zheng, G.J., Duan, F.K., Su, H., Ma, Y.L., Cheng, Y., Zheng, B., Zhang, Q., Huang, T., Kimoto, T., Chang, D., Poschl, U., Cheng, Y.F., He, K.B., 2015. Exploring the severe winter haze in Beijing: the impact of synoptic weather, regional transport and heterogeneous reactions. Atmos. Chem. Phys. 15, 2969–2983. https://doi.org/10.5194/acp-15-2969-2015.

Zhou, W., Tie, X., Zhou, G., Liang, P., 2015. Possible effects of climate change of wind on aerosol variation during winter in Shanghai, China. Particuology, Origin, evolution, and distribution of atmospheric aerosol particles in Asia 20, 80–88. https://doi.org/10.1016/j.partic.2014.08.008.

Zieger, P., Fierz-Schmidhauser, R., Poulain, L., Müller, T., Birmili, W., Spindler, G., Wiedensohler, A., Baltensperger, U., Weingartner, E., 2014. Influence of water uptake on the aerosol particle light scattering coefficients of the Central European aerosol. Tellus B 66, 22716. https://doi.org/10.3402/tellusb.v66.22716.